arXiv:2301.09040v1 [cond-mat.soft] 22 Jan 2023

Collective dynamics and shattering of disturbed two-dimensional Lennard-Jones crystals

Zhenwei Yao*
School of Physics and Astronomy, and Institute of Natural Sciences, Shanghai Jiao Tong University, Shanghai 200240, China

Elucidating collective dynamics in crystalline systems is a common scientific question in multiple fields. In this work, by combination of high-precision numerical approach and analytical normal mode analysis, we systematically investigate the dynamical response of two-dimensional Lennard-Jones crystal as a purely classical mechanical system under random disturbance of varying strength, and reveal rich microscopic dynamics. Specifically, we observe highly symmetric velocity field composed of sharply divided coherent and disordered regions, and identify the order-disorder dynamical transition of the velocity field. Under stronger disturbance, we reveal the vacancy-driven shattering of the crystal. This featured disruption mode is fundamentally different from the dislocation-unbinding scenario in two-dimensional melting. We also examine the healing dynamics associated with vacancies of varying size. The results in this work advance our understanding about the formation of collective dynamics and crystal disruption, and may have implications in elucidating relevant non-equilibrium behaviors in a host of crystalline systems.

I. INTRODUCTION

Understanding dynamical response of crystalline systems to external disturbance is a common scientific question arising in crystal stability [1–3], piezoelectric effect [4, 5], crystal melting [6–9], dynamic self-assembly [10–13], and various non-equilibrium phenomena [14–22]. Especially, the disruption of two-dimensional crystals under thermal agitation (melting) has been intensively studied in the past decades [6, 23–28], and continuum elasticity theory (KTHNY theory) based on dissociation of topological defects has been developed to explain two-dimensional crystal melting [6, 7, 29–32]. While it has been reported from the perspective of solid mechanics that instability with respect to a shearing deformation is crucial for the melting process [1], further investigation from the perspective of microscopic dynamics, which has not been fully carried out for the challenge in direct observation of the phase transition of atomic or molecular materials, may yield new insights into the fundamental inquiries into the crystal disruption phenomenon in general [33]. To this end, the model system of Lennard-Jones (L-J) crystal, as fabricated by particles interacting under the L-J potential, provides a suitable platform [34–36]. The L-J potential has been extensively employed to simulate interatomic interactions since 1924 [37].

The goal of this work is to explore the dynamical response of the two-dimensional L-J crystal system to random disturbance of varying strength, focusing on the stimulated collective dynamics and the disruption of the crystal. Specifically, we disturb the system by imposing a random displacement on each particle. In this work, the L-J lattice is treated as a purely classical mechanical system. The evolution of the system conforms to deterministic Hamiltonian dynamics. A suitable approach to exploring the dynamics of L-J crystals is by high-precision numerical integration of the equations of motion in combination with theoretical analysis of normal modes [38, 39]. This approach allows us to explore the regime of large disturbance beyond the scope of harmonic analysis [39–42]. The L-J crystal system provides an opportunity to clarify a host of questions with broad implications, such as: Will the random disturbance lead to coherent dynamical states? If yes, under which conditions, and which kinds of collective modes will be excited? How will the crystalline order be disrupted upon strong disturbance? Previous studies have shown that geometrically frustrated L-J crystals can support dislocational and disclinational vacancies due to the steep energy minimum in the L-J potential curve [36]. It implies a vacancy-driven disruption scenario in the L-J crystal system that is distinct from the dislocation-unbinding mechanism in the melting of two-dimensional crystals [6, 7].

In this work, we reveal rich microscopic dynamics of two-dimensional L-J crystal under the disturbance of random orientation and given amplitude. In the perturbation regime, we find that the velocity field exhibits various featured patterns composed of sharply divided coherent and disordered regions; the degree of orderness is characterized by a dynamical order parameter. Remarkably, the symmetry of the temporally-varying velocity field is well preserved in the dynamical evolution of the system. Analytical normal mode analysis suggests that the disordered region originates from the singularity structure in the velocity field. By increasing the disturbance amplitude, the velocity field experiences a dynamical transition towards a completely disordered state. Under larger disturbance amplitude (about 10% of the lattice spacing), we track the dynamical disruption process, and reveal the vacancy-driven shattering of the crystal. The finite size effect and stress-free boundary condition are crucial for shaping such a featured disruption mode.

*zyao@sjtu.edu.cn

We also examine the healing dynamics associated with vacancies of varying size. This work reveals rich dynamics in the L-J model system under random disturbance, and may have implications in elucidating intriguing non-equilibrium behaviors in a host of crystalline systems.

II. MODEL AND METHOD

The model consists of a collection of point particles confined on the plane interacting via the L-J potential V_{LJ}. In the initial configuration, the particles constitute a triangular lattice with given boundary shape. The lattice spacing is set to be the balance distance r_m of the L-J potential. No external stress is applied on the boundary. Note that the equilibrium lattice spacing in a finite L-J crystal is slightly smaller than r_m due to the line tension. We disturb the system by imposing a random displacement $\delta\vec{x}$ on each particle. $\delta\vec{x} = br_m(\cos\alpha, \sin\alpha)$ in the Cartesian coordinates. The magnitude and direction of the disturbance is specified by br_m and α, respectively. α is a uniform random variable in $[0, 2\pi)$. b is a key controlling parameter, and its value is specified in percentage form. The ensuing evolution of the system is governed by the Hamiltonian:

$$H = \sum_{i=1}^{N} \frac{\vec{p}_i^2}{2m_0} + \sum_{i\neq j} V_{LJ}(||\vec{x}_i - \vec{x}_j||), \tag{1}$$

where $V_{LJ}(r) = 4\epsilon_0[(\sigma_0/r)^{12} - (\sigma_0/r)^6]$. The balance distance $r_m = 2^{1/6}\sigma_0$. We numerically solve the $2N$ coupled equations of motion derived from eqn (1). Specifically, we employ the Verlet method to construct high-quality particle trajectories with well conserved total energy, momentum and angular momentum as well as fixed center of mass for up to a million simulation steps (see SI for technical details) [38]. This first-principle approach allows us to explore the nonlinear regime of large disturbance and investigate in detail the microscopic dynamics of crystal disruption. In this work, the units of length, mass, and time are r_m, m_0, and τ_0, respectively. $\tau_0 = r_m\sqrt{m_0/\epsilon_0}$.

III. RESULTS AND DISCUSSION

A. Preliminary analysis of elementary hexagonal configurations

We first consider the analytically tractable cases of 6- and 7-particle hexagonal configurations as shown in Fig. 1, and analyze the normal modes in the perturbation regime, where the interaction between neighboring particles is approximated by the harmonic potential. These two kinds of elementary hexagonal configurations are denoted as H_6 and H_7. We analytically derive for all of the normal modes and their frequencies from the eigenvalue equations [39]:

$$(V_{ij} - T_{ij}\omega_k^2)a_{jk} = 0, \tag{2}$$

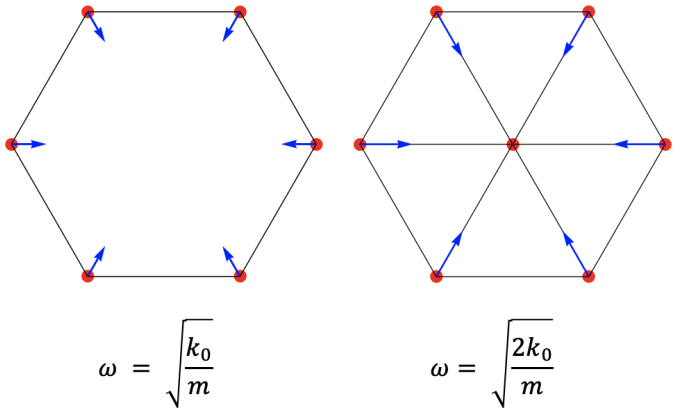


FIG. 1: Radial normal modes in the hexagonal 6- and 7-particle configurations H_6 and H_7 that are compatible with the C_6 symmetry of the system. The black bonds represent springs with stiffness k_0. In the H_6 configuration (the right panel), the radial mode has the lowest frequency among all the normal modes. In the H_7 configuration, the eigenfrequency of the radial mode is identical to that of the harmonic oscillator system consisting of two spring-connected mass points.

where V_{ij} and T_{ij} are the matrices related to the potential and kinetic energies. ω_k and a_{jk} are the frequency and eigenvector of the k-mode. The complete results and derivation details are presented in SI. In all of the normal modes, the total momentum and angular moment are conserved, and the center of mass is invariant in time.

In the extension of the system from the elementary hexagonal configurations to a large triangular lattice of hexagonal shape, the analysis of the normal modes in the H_6 and H_7 configurations inspires a series of inquiries. First of all, among all of the normal modes, it is found that only the radial modes shown in Fig. 1 possesses the C_6 symmetry. Will this symmetry be preserved in the large system? In general, will the velocity field as a whole respect the symmetry of the boundary? Furthermore, for the radial mode in the H_7 case, it is noticed that the velocity of the central particle is zero. Does it imply the appearance of a singularity point in the velocity field in the continuum limit? If yes, will the singularity structure in the velocity field manifest itself as a point or other dynamical morphologies? It is also noticed that the frequency of the radial mode in the H_6 configuration is smaller than that in the H_7 configuration due to the vacancy at the center of the H_6 system; in fact, the radial mode has the lowest frequency among all the normal modes in the H_6 configuration (see SI). According to Maxwell's rule regarding the stability of a mechanical structure, removing the central particle in the H_7 configuration leads to floppy modes in the resulting H_6 configuration, and thus fundamentally changes the dynamical state of the system [43, 44]. It is therefore of interest to examine the vacancy-related dynamics in a large lattice.

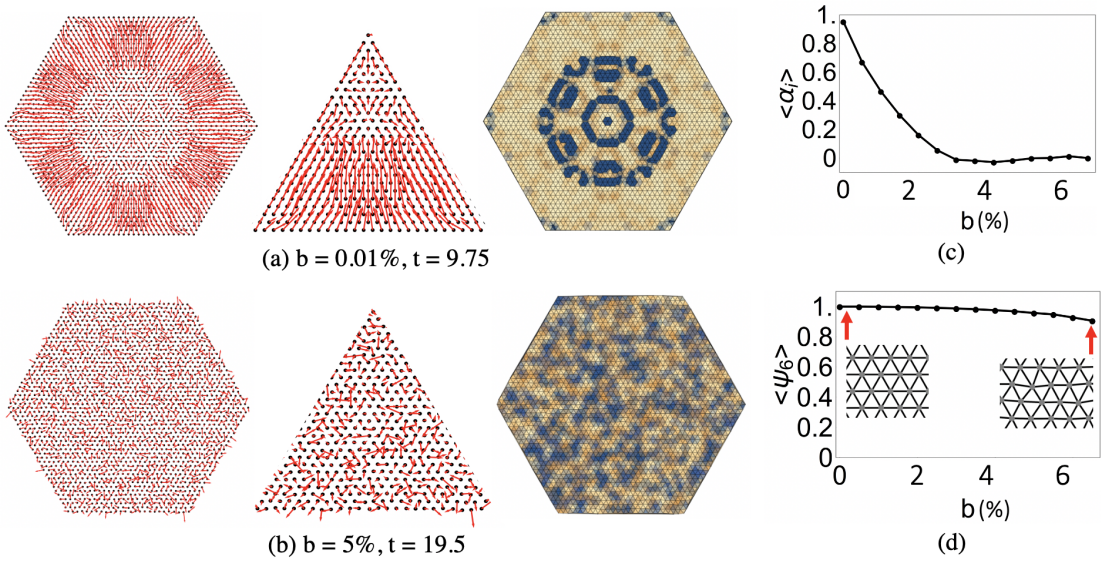


FIG. 2: Random disturbance driven dynamical transition in the velocity field of a triangular lattice of L-J particles with hexagonal shape and stress-free boundary condition. (a) Coexistence of coherent and disordered regions at the disturbance amplitude of $b = 0.01\%$. The particle velocity is represented by the red arrows. Remarkably, the velocity field maintains the C_6 symmetry in the evolution of ever-changing pattern. (b) Disordered state at $b = 5\%$. The panels in the third column are the $\alpha-$fields. The dynamical order parameter α_i measures the correlation of the velocity of particle i and the average velocity of its neighboring particles. The value of α_i is larger in the brighter region. (c) Plot of the spatiotemporally averaged dynamical order parameter α_i versus b. (d) Plot of the spatiotemporally averaged ψ_6 versus b. ψ_6 characterizes the bond-orientational order of the lattice. The spatiotemporal averaging of both α_i and ψ_6 is over the entire system during the time interval of $100\tau_0$. More instantaneous velocity fields are presented in SI. $N = 1951$.

B. Formation of collective dynamics and dynamical transition in the disturbed crystal

To address the questions proposed in the preceding subsection, we first resort to high-precision numerical integration of the equations of motion to construct high-quality particle trajectories with well conserved total energy, momentum and angular momentum.

In a disturbed triangular lattice of hexagonal shape, we observe that individual motions of the particles are quickly (in comparison with the characteristic time τ_0) organized to form coherent dynamical states. A typical instantaneous velocity field for $b = 0.01\%$ (measured in the unit of the lattice spacing r_m) is presented in Fig. 2(a) for a system of 1951 particles. We see that the entire velocity field exhibits C_6 symmetry that is consistent with the crystal boundary. Remarkably, the velocity field maintains the C_6 symmetry in the evolution of the ever-changing pattern. We also investigate the case of rectangular boundaries, and find that the boundary symmetry also dictates the symmetry of the velocity field. Typical instantaneous velocity fields of rectangular crystals are presented in SI.

A salient common feature of the velocity field driven by random perturbation is that the velocity vectors exhibit distinct behaviors in different regions, as shown in Fig. 2(a). A zoomed-in plot of a sixth of the entire $\vec{v}$-field is shown in the second panel. In some region, the motions of the particles follow the average orientation of the neighboring velocity vectors. In the remaining region, the orientations of adjacent velocity vectors seem uncorrelated. To quantify the distinct behaviors of the velocity vectors, we introduce a dynamical order parameter α_i defined at particle i:

$$\alpha_i = \frac{\vec{v}_i \cdot \langle \vec{v}_j \rangle}{\|\vec{v}_i\| \cdot \|\langle \vec{v}_j \rangle\|}. \tag{3}$$

$\langle \vec{v}_j \rangle$ is the average velocity of the neighboring particles of particle i; the neighbors of a particle are determined by the standard Delaunay triangulation [7]. $\langle \vec{v}_j \rangle = \frac{1}{n_i} \sum_{j=1}^{n_i} \vec{v}_j$, where n_i is the coordination number of particle i. When $\vec{v}_i$ follows the orientation of $\langle \vec{v}_j \rangle$, $\alpha_i = 1$, and the cluster of the particles tends to move coherently. The order parameter α_i thus characterizes the local alignment of velocity vectors regardless of their magnitude.

In the third panel in Fig. 2(a), we show the instantaneous α-field with C_6 symmetry. In the brighter region, the value of α is larger. The α-field clearly shows that the velocity field is sharply divided into ordered (bright) and disordered (dark) regions. Here, we shall note that the degree of order in the velocity field is specified by the value of the order parameter α_i as defined in eqn (3); the system is still in the crystalline state under mild disturbance. Extensive data analysis of both hexagonal and rectangular systems shows that the coexistence of ordered and disordered regions is a common feature of the

velocity field in the perturbation regime. Our proposal of the dynamical order parameter α_i is inspired by the seminal work of active matter physics, where the rule of specifying particle velocity by the average velocity of surrounding particles has been employed to create coherent collective dynamics [14].

The origin of the disordered region in the velocity field is closely related to the key observation that the boundary particles tend to move perpendicular to the boundary. Such a boundary dynamical state leads to a nonzero winding number in the interior velocity vector field [45]. Consequently, singularities are inevitable in the interior velocity field. The disordered region in the velocity field may be regarded as an area full of singularities in the continuum limit. In contrast, by fixing the positions of the boundary particles, our simulations show that the entire velocity field becomes disordered everywhere. Note that the disordered region in the velocity field of the disturbed L-J lattice is distinct from the node structure arising in standing waves.

With the increase of the disturbance amplitude, we observe the dynamical transition of the velocity field from the coexistence of ordered and disordered regions to completely disordered state. In Fig.2(b), we show that when the value of b increases to 5% of the lattice spacing, both the velocity vectors and the α-field become disordered. We characterize this dynamical transition in the plot of $\langle\alpha_i\rangle$ versus b in Fig.2(c). $\langle\alpha_i\rangle$ is the spatiotemporal averaging of the order parameter α_i over tens of instantaneous velocity fields during the time interval of $100\tau_0$. From Fig.2(c), we see that the velocity field becomes completely disordered ($\langle\alpha_i\rangle = 0$) when the amplitude of disturbance exceeds about 2% of the lattice spacing. Dynamical transition is also reflected in the kinetic energy curves: the originally periodic energy curve becomes irregular at short time scale when dynamical transition occurs (more information about the energy curves is presented in SI).

Here, we shall emphasize that the crystalline order is still well preserved in the dynamical transition of the velocity field in preceding discussions. The lattice becomes slightly wiggly with the increasing disturbance strength. The resulting variation of the bond-orientational order of the lattice can be quantified by the order parameter $\psi_6(\vec{x}_i)$ [46]:

$$\psi_6(\vec{x}_i) = \frac{1}{n_i}\sum_{j=1}^{n_i} e^{i6\theta_j}, \tag{4}$$

where θ_j is the angle of the bond connecting the particle i and its neighbor j with respect to some chosen reference line. n_i is the coordination number of the particle i. From Fig.2(d), we see the slight decline of the spatiotemporally averaged ψ_6 with the increase of b, indicating that the crystalline order is well preserved up to $b \approx 6\%$.

C. Vacancy-driven shattering of the crystal under strong disturbance

We proceed to explore the regime of stronger disturbance. At $b \approx 7\%$, we observe the transient existence of a few quadrupoles in the crystal. The bond-orientational order is still preserved. A schematic plot of a quadrupole is shown in the right panel in Fig. 3(h). The red and blue dots represent five- and seven-fold disclinations, which are elementary topological defects in two-dimensional triangular lattices. An n-fold disclination in triangular lattice is a vertex whose coordination number n is deviated from six. The coordination number of a particle can be uniquely determined by the standard Delaunay triangulation [7]. One may define the topological charge of an n-fold disclination as $q_i = (6-n)\pi/3$. Topological charges of the same sign repel and those of opposite signs attract, which resembles the behavior of electric charges [7]. A pair of five- and seven-fold disclinations form a dislocation. And a pair of dislocations form a quadrupole as shown in Fig. 3(h). While the emergence of an isolated disclination requires a global reconfiguration of the particle array, a quadrupole can be excited by a slight local compression of the particles indicated by the red arrows in Fig. 3(h). Energetically, it required much less energy to excite a quadrupole than either a dislocation or a disclination [47].

According to the elegant KTHNY theory, the disruption of two-dimensional crystals under thermal agitation (melting) involves the consecutive solid-hexatic and hexatic-liquid transitions [6, 7]. The intermediate hexatic phase is characterized by the proliferation of dislocations which still preserves the bond-orientational order; the dislocation-unbinding transition leads to the isotropic liquid phase.

Here, for our L-J crystal system of finite size under the stress-free boundary condition, we discover the featured vacancy-driven disruption mode that is distinct from the dislocation-unbinding mechanism in the melting of two-dimensional crystals. Typical particle configurations for $b = 8\%$ and 10% are presented in Figs. 3(a)-3(d) and 3(e)-3(g), respectively. Simulations show that the disruption of the crystalline order is initiated from the center of the system. For clarity, only the central circular regions of the hexagonal crystals are shown in Fig. 3. For the case of $b = 8\%$, we observe the unbinding of the quadrupole into a pair of dislocations [see Fig. 3(b)], and the appearance of void regions (bubbles) extending several lattice spacings [see Fig. 3(c)]. Line tension emerges once a bubble is formed, and it tends to inhibit the growing of the bubble. At the disturbance amplitude of $b = 8\%$, the line-tension effect wins, and we observe the closure of the bubbles, resulting in different kinds of vacancies [see Fig. 3(d); also see SI] [36].

By increasing the disturbance amplitude to $b = 10\%$, we find that the line tension fails to suppress the growing of the bubbles, and the entire crystal is shattered into several pieces of crystallites, as shown in Fig. 3(e)-

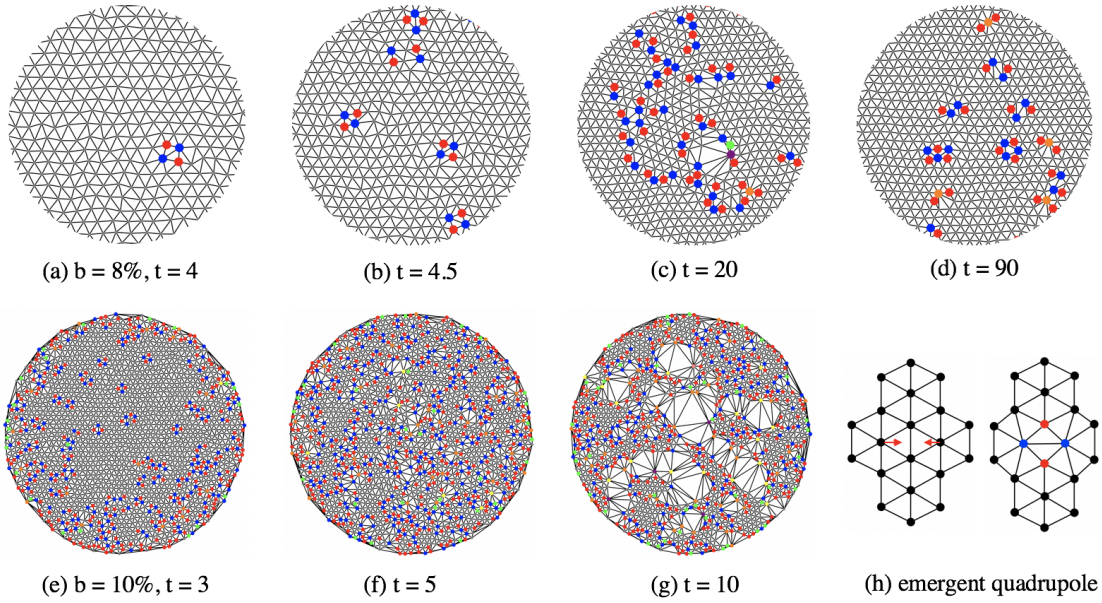


FIG. 3: Disruption of the crystalline order in a triangular lattice of L-J particles with hexagonal shape and stress-free boundary condition under random disturbance. The central circular region of the hexagonal crystals of instantaneous particle configurations are shown for clarity. The green, red, blue, and orange dots represent four-, five-, seven- and eight-fold disclinations, respectively. We observe the sequential emergence of quadrupoles, dislocations and void regions (bubbles) in the disturbed lattice. Competition of the line tension and the disturbance strength leads to the closure of the bubbles at $b = 8\%$ (d) and the shattering of the entire crystal into pieces of crystallites at $b = 10\%$ (g). (h) Illustration of the formation of a quadrupole. $N = 1951$.

3(g). It is noticed that the critical value of the disturbance amplitude ($b = 10\%$) for the mechanical disruption of the two-dimensional L-J lattice agrees with both the conventional Lindemann melting criterion for three-dimensional solid [48] and the modified Lindemann's criterion for two-dimensional solid [28, 49]. The conventional Lindemann's criterion states that melting of three-dimensional solid occurs when the square root of the particle mean-squared displacement from the equilibrium position reaches a threshold value of about one tenth of the interparticle distance [48]. This criterion is generalized to two-dimensional solid by measuring the displacements of particles in local coordinate [28, 49]. Here, we shall emphasize that in our work the L-J crystal is two-dimensional, and it is treated as a purely classical mechanical system whose evolution conforms to deterministic Hamiltonian dynamics. The Lindemann's criterion is applicable to the melting of solid as a thermodynamic system [28, 49].

In contrast, under periodic boundary condition, simulations of L-J systems show the existence of a metastable state between the solid and liquid phases [50], and the featured defect fraction as predicted by the KTHNY theory [51]. Furthermore, for the case of a hexagonal L-J crystal with fixed boundary, our simulations show that the constraint of fixed area suppresses the development of bubble structures, and the disruption process resembles the melting scenario of two-dimensional crystals according to the KTHNY theory (more information is presented in SI). To conclude, the disruption of the two-dimensional L-J crystal occurs in the form of the vacancy-driven shattering under the stress-free boundary condition, which is in contrast to the dislocation-unbinding mechanism (the

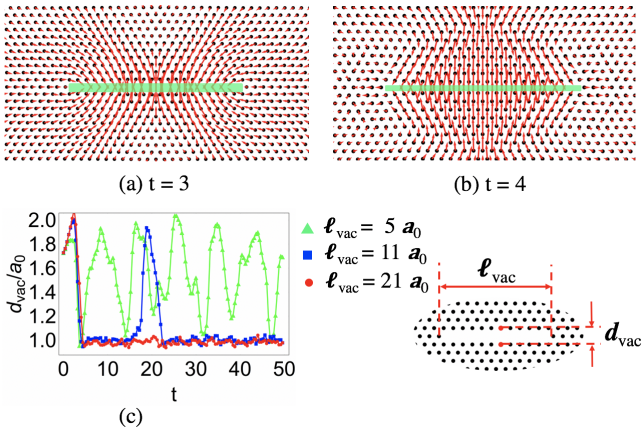


FIG. 4: Healing dynamics in a triangular lattice of L-J particles with hexagonal shape and stress-free boundary condition. An n-point linear vacancy is created at the center (indicated by light green bars). For visual convenience, only the velocity field near the vacancy is shown. (a) and (b) Plots of instantaneous velocity field prior to the closure of the vacancy. (c) Plot of the vacancy width d_{vac} versus time at varying vacancy length ℓ_{vac}. The local particle configuration near the n-point vacancy is shown in the lower right panel. $b = 0$. $N = 1951$.

scenario of the KTHNY theory) at constant density as implemented by either the periodic boundary condition or the fixed boundary condition.

Fluctuation of the bubble structure in its size inspires us to ask how a void region is healed under line tension. To address this question, we create an n-point linear vacancy at the center of a hexagonal L-J crystal simply by removing n particles. Typical instantaneous velocity fields prior to the closure of the n-point vacancy are shown in Figs. 4(a) and 4(b). The particles near the vacancy move coherently to shrink the width $d_{\rm vac}$ of the linear vacancy as indicated by the light green bar. Here, the introduction of the linear vacancy breaks the C_6 symmetry of the system. The symmetry of the resulting velocity field changes accordingly. We track the temporally-varying vacancy width $d_{\rm vac}$ at varying vacancy length $\ell_{\rm vac}$ (without imposing any disturbance), and the results are presented in Fig. 4(c). It turns out that the short- and long-vacancies exhibit distinct dynamical behaviors. The short vacancy ($\ell_{\rm vac} = 5a_0$) alternately opens and closes. In contrast, the long vacancy ($\ell_{\rm vac} = 21a_0$) is quickly healed, leaving out a pair of dislocations at its two ends with opposite Burgers vectors. Note that our previous molecular dynamics simulations have shown that infinitely large two-dimensional L-J crystal exhibits similar behaviors [35]. For the intermediate case of $\ell_{\rm vac} = 11a_0$, our numerical solution captures the transient open state of the vacancy for a duration of $\Delta t \approx 11$ [see the blue curve in Fig. 4(c)]. By imposing perturbation, the $d_{vac}(t)$ curves at varying vacancy size for $b = 1\%$ are almost identical with those in Fig. 4(c).

IV. CONCLUSION

In summary, in this work we have explored the random disturbance driven microscopic dynamics in the L-J crystal system. In the perturbation regime, we observed the symmetry-preserved velocity field consisting of sharply divided coherent and disordered regions. Under stronger disturbance, we identified the dynamical transition, and revealed the featured vacancy-driven disruption of crystal in the form of shattering. We also discussed the healing dynamics associated with vacancies of varying size. An important observation in our study is the crucial role of the boundary condition for shaping the collective dynamics and the disruption mode. Specifically, under the stress-free boundary condition, the boundary particles tend to move perpendicular to the boundary, which is responsible for both the preservation of the symmetry and the formation and evolution of the singularity structure in the velocity field. The stress-free boundary condition also allows the system to develop the bubble structure, which is closely related to the shattering of the crystal. These results advance our understanding about collective dynamics and crystal disruption, and may have implications in elucidating intriguing dynamical non-equilibrium behaviors in a host of crystalline systems.

Acknowledgements

This work was supported by the National Natural Science Foundation of China (Grants No. BC4190050).

[1] M. Born, Math. Proc. Cambridge Philos. Soc. **36(2)**, 160 (1940)
[2] P. Řehak, M. Cerný, J. Pokluda, J. Phys.: Condens. Matter **24**(21), 215403 (2012)
[3] N.F.M. Holm Altenbach (ed.), *Surface Effects in Solid Mechanics: Models, Simulations and Applications* (Springer, 2013)
[4] T. Ikeda, *Fundamentals of Piezoelectricity* (1990)
[5] B.A. Auld, *Acoustic Fields and Waves in Solids* (Krieger Pub Co, 1990)
[6] K.J. Strandburg, Rev. Mod. Phys. **60**, 161 (1988)
[7] D.R. Nelson, *Defects and Geometry in Condensed Matter Physics* (Cambridge University Press, Cambridge, 2002)
[8] S.R. Williams, P. Mcglynn, G. Bryant, I.K. Snook, W. Van Megen, Phys. Rev. E **74**(3), 031204 (2006)
[9] U. Gasser, C. Eisenmann, G. Maret, P. Keim, ChemPhysChem **11**(5), 963 (2010)
[10] B.A. Grzybowski, H.A. Stone, G.M. Whitesides, Nature **405**(6790), 1033 (2000)
[11] A. Grinthal, S.H. Kang, A.K. Epstein, M. Aizenberg, M. Khan, J. Aizenberg, Nano Today **7**(1), 35 (2012)
[12] M. Matsunaga, M. Aizenberg, J. Aizenberg, J. Am. Chem. Soc. **133**(14), 5545 (2011)
[13] Y. Suzuki, G. Cardone, D. Restrepo, P.D. Zavattieri, T.S. Baker, F.A. Tezcan, Nature **533**(7603), 369 (2016)
[14] T. Vicsek, A. Czirók, E. Ben-Jacob, I. Cohen, O. Shochet, Phys. Rev. Lett. **75**(6), 1226 (1995)
[15] D. Helbing, I. Farkas, T. Vicsek, Nature **407**(6803), 487 (2000)
[16] A.S. Smith, Nature Physics **6**(10), 726 (2010)
[17] P.C. Davies, L. Demetrius, J.A. Tuszynski, Theor. Biol. Med. Modell. **8**(1), 30 (2011)
[18] M. Marchetti, J. Joanny, S. Ramaswamy, T. Liverpool, J. Prost, M. Rao, R.A. Simha, Rev. Mod. Phys. **85**(3), 1143 (2013)
[19] F.C. Keber, E. Loiseau, T. Sanchez, S.J. DeCamp, L. Giomi, M.J. Bowick, M.C. Marchetti, Z. Dogic, A.R. Bausch, Science **345**(6201), 1135 (2014)

[20] R. Sknepnek, S. Henkes, Phys. Rev. E **91**(2), 022306 (2015)
[21] Z. Yao, Soft Matter **12**(33), 7020 (2016)
[22] A.V. Zampetaki, B. Liebchen, A.V. Ivlev, H. Löwen, Proc. Natl. Acad. Sci. U.S.A. **118**(49) (2021)
[23] S. Toxvaerd, J. Chem. Phys. **69**(11), 4750 (1978)
[24] J. Barker, D. Henderson, F.F. Abraham, Physica A **106**(1-2), 226 (1981)
[25] S. Toxværd, Phys. Rev. Lett. **51**(21), 1971 (1983)
[26] A.Z. Patashinski, R. Orlik, A.C. Mitus, B.A. Grzybowski, M.A. Ratner, J. Phys. Chem. C **114**(48), 20749 (2010)
[27] Y.W. Li, M.P. Ciamarra, Phys. Rev. E **102**(6), 062101 (2020)
[28] S.A. Khrapak, Physical Review Research **2**(1), 012040 (2020)
[29] J.M. Kosterlitz, D.J. Thouless, J. Phys. C: Solid State Phys. **6**(7), 1181 (1973)
[30] A. Young, Phys. Rev. B **19**(4), 1855 (1979)
[31] D.R. Nelson, B. Halperin, Phys. Rev. B **19**(5), 2457 (1979)
[32] M. Zu, J. Liu, H. Tong, N. Xu, Phys. Rev. Lett. **117(8)**, 085702 (2016)
[33] H. Hwang, D.A. Weitz, F. Spaepen, Proc. Natl. Acad. Sci. U.S.A. **116**(4), 1180 (2019)
[34] J.N. Israelachvili, *Intermolecular and Surface Forces*, 3rd edn. (Academic Press, New York, 2011)
[35] Z. Yao, M. Olvera de la Cruz, Phys. Rev. E **90**(6), 062318 (2014)
[36] Z. Yao, Soft Matter **13**(35), 5905 (2017)
[37] J.E. Jones, Proceedings of the Royal Society of London. Series A **106**(738), 463 (1924)
[38] D. Rapaport, *The Art of Molecular Dynamics Simulation* (Cambridge University Press, Cambridge, UK, 2004)
[39] H. Goldstein, *Classical Mechanics* (Pearson Education India, 2011)
[40] N. Xu, M. Wyart, A.J. Liu, S.R. Nagel, Phys. Rev. Lett. **98**(17), 175502 (2007)
[41] A. Vallés, P. Derlet, D. Crespo, E. Pineda, J. Alloys Compd. **586**, S250 (2014)
[42] Z. Yao, Phys. Rev. Lett. **122**(22), 228002 (2019)
[43] J.C. Maxwell, Philos. Mag. **27**(182), 294 (1864)
[44] V. Vitelli, PNAS **109**(31), 12266 (2012)
[45] Y. Aminov, *Geometry of vector fields* (CRC Press, 2000)
[46] R. Bruinsma, D. Nelson, Phys. Rev. B **23**(1), 402 (1981)
[47] P. Chaikin, T. Lubensky, *Principles of Condensed Matter Physics* (Cambridge University Press, 1995)
[48] F. Lindemann, Z. Phys. **11**, 609 (1910)
[49] X. Zheng, J. Earnshaw, Europhys. Lett. **41**(6), 635 (1998)
[50] K. Chen, T. Kaplan, M. Mostoller, Phys. Rev. Lett. **74**(20), 4019 (1995)
[51] K. Wierschem, E. Manousakis, Phys. Rev. B **83**(21), 214108 (2011)